

# Coagulation drives turbulence in binary fluid mixtures

Akshay Bhatnagar,<sup>1,\*</sup> Prasad Perlekar,<sup>2,†</sup> and Dhrubaditya Mitra<sup>1,‡</sup>

<sup>1</sup>*Nordita, KTH Royal Institute of Technology and Stockholm University, Roslagstullsbacken 23, 10691 Stockholm, Sweden*

<sup>2</sup>*TIFR Centre for Interdisciplinary Sciences, Tata Institute of Fundamental Research, Gopanpally, Hyderabad 500046, India.*

We use direct numerical simulations and scaling arguments to study coarsening in binary fluid mixtures with a conserved order parameter in the droplet-spinodal regime – the volume fraction of the droplets is neither too small nor symmetric – for small diffusivity and viscosity. Coagulation of droplets drives a turbulent flow that eventually decays. We uncover a novel coarsening mechanism, driven by turbulence where the characteristic length scale of the flow is different from the characteristic length scale of droplets, giving rise to a domain growth law of  $t^{1/2}$ , where  $t$  is time. At intermediate times, both the flow and the droplets form self-similar structures: the structure factor  $S(q) \sim q^{-2}$  and the kinetic energy spectra  $E(q) \sim q^{-5/3}$  for an intermediate range of  $q$ , the wavenumber.

The non-equilibrium dynamics of phase separation plays a crucial role in many different branches of physics, e.g., in condensed matter systems [1–7] both classical and quantum [8–10], nuclear matter [11], cosmology [12], and astrophysics [13, 14]. To set the scene, consider the canonical model of equilibrium phase transition: the Landau-Ginzburg type  $\phi^4$  theory with a scalar order-parameter  $\phi$  [2]. We show a sketch of its equilibrium phase diagram in Fig. (1A). When the system is quenched from an uniform high-temperature phase to a state below the coexistence curve the uniform phase is no longer in stable thermal equilibrium. The system approaches equilibrium – two co-existing domains with  $\phi = 1$  and  $\phi = -1$  separated by a domain wall – by phase separating. We consider the case where the order parameter is conserved – *model B* of Hohenberg and Halperin [1]. If the thermal noise is ignored – which is the case in the rest of this paper – *model B* reduces to the Cahn-Hilliard equation [15]. Domain growth in the Cahn-Hilliard equations shows a variety of dynamical behavior that has been uncovered by analytical and numerical techniques [see e.g., 2, 4, 5, 16].

In binary fluid mixtures, e.g., oil-water systems, flows are also coupled with the phase separation dynamics – the Cahn-Hilliard-Navier-Stokes equations or the *model H* of Hohenberg and Halperin without noise. There are a plethora of possible growth mechanisms and corresponding growth laws [7] that have been investigated: (a) diffusive growth, essentially by the Lifshitz-Slyozov-Wagner mechanism [17, 18] that operates in *model B*; (b) collisional growth due to Brownian motion of the droplets [19–22]; (c) growth due to the viscous flows [20]; and (d) growth due to inertial flows [23–25]. The mechanisms (a) and (b) give the growth law  $L \sim t^{1/3}$ ; (c) gives  $L \sim t$ ; and (d)  $L \sim t^{2/3}$ . Furthermore coarsening also depend on initial condition – whether it is a critical quench (inside the spinodal curve) or an off-critical

quench (near the phase-coexistence curve) [26–28]. The possible growth mechanisms and the growth laws have been extensively studied experimentally too [29–32]. Dynamics of domain growth near the co-existence line and well inside the spinodal for not too small diffusivity and viscosity are reasonably well understood.

Due to the necessity of massive computational resources, the part of parameter space with small diffusivity and viscosity remained unexplored. Recently, Naso and Naráigh [33], for the first time, obtained signatures of novel coarsening behavior in this regime. In this paper, we lay bare the growth-laws and the turbulent flows that develop in this regime using scaling theory and analysis of the largest direct numerical simulations of the Cahn-Hilliard-Navier-Stokes equations. In particular, we show that if the system is initialised in the droplet-spinodal regime [28] coagulation of droplets drive a nonlinear flux of kinetic energy that gives rise to Kolmogorov-like turbulence and a scaling of  $L \sim t^{1/2}$  at intermediate times. We also present a scaling theory of this phenomena.

The Cahn-Hilliard-Navier-Stokes equations are given by:

$$\partial_t \phi + \nabla \cdot \mathbf{J} = 0 \quad . \quad (1a)$$

$$\mathbf{J} = \mathbf{v}\phi - \Gamma \nabla \mu \quad . \quad (1b)$$

$$\mu = \frac{\delta \mathcal{F}}{\delta \phi} \quad . \quad (1c)$$

$$\mathcal{F}[\phi] = \frac{\Lambda}{\xi^2} \int d^d x \left[ f(\phi) + \frac{\xi^2}{2} |\nabla \phi|^2 \right] \quad . \quad (1d)$$

$$f(\phi) = \frac{1}{4} (1 - \phi^2)^2 \quad . \quad (1e)$$

$$\rho(\partial_t + \mathbf{v} \cdot \nabla) \mathbf{v} = \eta \nabla^2 \mathbf{v} - \rho \nabla p - \phi \nabla \mu. \quad (1f)$$

$$\nabla \cdot \mathbf{v} = 0. \quad (1g)$$

Here  $\phi$  is the order-parameter,  $\mathbf{v}$  the velocity of the flow,  $\mu$  the chemical potential,  $\Gamma$  the transport coefficient of the chemical potential,  $\eta = \rho\nu$  is the dynamic viscosity,  $\rho$  is the density,  $\nu$  the kinematic viscosity, and  $\xi$  is the length-scale that characterizes the interface thickness. The surface tension  $\sigma = (2\sqrt{2}/3)\Lambda/\xi$

\* akshayphy@gmail.com

† perlekar@tifrh.res.in

‡ dhruba.mitra@gmail.com

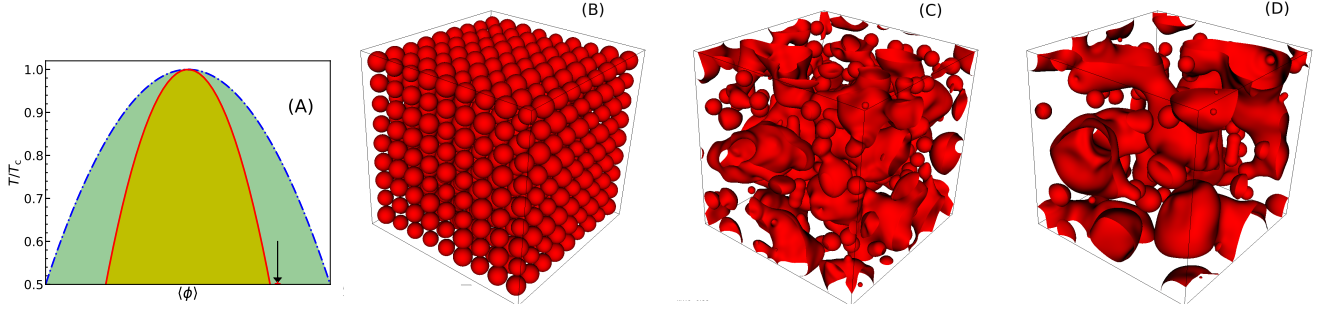


FIG. 1. (A) A sketch of the phase-diagram of Landau-Ginzburg type  $\phi^4$  theory. The blue dashed line is the phase coexistence curve. The red line is the spinodal curve. Near the phase coexistence line droplets form by nucleation. Inside the red line domains grow by spinodal decomposition. The point marked by a red star, pointed at by the arrow, shows our position in this phase-diagram; this is outside the spinodal curve but not too close to the phase coexistence line – droplet spinodal decomposition operates here. (B), (C), (D): Isosurfaces of  $\phi$  at  $\phi = 0$  for  $La = 10^5$  at times  $\tau = 0, 18,$  and  $35$  respectively.

We use the initial size of the droplets  $R$  as the characteristic length scale and  $V = \nu/R$  as the characteristic velocity. The non-dimensional parameters are the Laplace number  $La \equiv \sigma R/(\rho\nu^2)$ , the Schmidt number  $Sc \equiv \nu/D$ , and the Cahn number  $Ch \equiv \xi/R$ , where the diffusivity  $D \equiv \Gamma\Lambda/\xi^2$ . In all our simulations  $Sc = 1$  and we use several Laplace numbers and two different Cahn numbers. We use a spectral code with periodic boundary conditions with  $N^3$  resolutions where  $N = 512$  and  $1024$  – the highest resolution simulations done for this system [34].

We choose all the droplets to have the same radius  $R/L = 1/(8\pi)$  and their centers placed on a cubic lattice. We then add small random perturbations to the radii of the droplets, see Fig. (1B). The initial volume fraction occupied by the droplets (minority phase) is approximately 0.2 such that  $\langle\phi\rangle = 0.62$ , where  $\langle\cdot\rangle$  denotes spatial averaging. This choice of  $\langle\phi\rangle$ , marked in the phase-diagram, Fig. (1A), puts us in the droplet spinodal decomposition regime [28] – we are neither well inside the spinodal curve nor very close to the co-existence curve.

We show how coarsening progresses in Fig. (1B) to Fig. (1D). At very early times the drops remains practically unchanged in size but move – typically towards their closest neighbour. At  $t = 0$  there was no flow – the flows that move the droplets are generated by compositional Marangoni effect [28]. To confirm, we simulate a collection of seven drops - one central drop at the origin and six drops placed on a cubic lattice around it. Due to the asymmetry all the peripheral drops move towards the central drop and eventually merge into one. A similar experiment where we place the drops on a line also show that drops move toward their nearest neighbours.

We define the structure factor and the energy spectrum as the shell-integrated Fourier spectra of  $\phi$  and  $\mathbf{v}$

respectively, i.e.,

$$\mathbb{S}(q) \equiv \int \hat{\phi}(\mathbf{q})\hat{\phi}(-\mathbf{q})d\Omega \quad , \quad (2a)$$

$$\mathbb{E}(q) \equiv \int \hat{\mathbf{v}}(\mathbf{q})\hat{\mathbf{v}}(-\mathbf{q})d\Omega \quad , \quad (2b)$$

where  $\hat{\phi}(\mathbf{q})$  and  $\hat{\mathbf{v}}(\mathbf{q})$  are respectively the Fourier transforms of  $\phi(\mathbf{x})$  and  $\mathbf{v}(\mathbf{x})$ ,  $q = |\mathbf{q}|$  is the magnitude of the wavevector  $\mathbf{q}$ , and  $\Omega$  is the solid angle in Fourier space. We calculate the evolving, characteristic length scale,  $L$  as [28, 35]

$$K \equiv \frac{\int dq q \mathbb{S}(q)}{\int dq \mathbb{S}(q)} \quad \text{and} \quad L \equiv 2\pi/K \quad (3)$$

The time evolution of the characteristic length scale  $L(t)$  and the total kinetic energy  $E(t)$  are shown in Fig. (2). The evolution for different Laplace numbers collapse when plotted as a function of scaled dimensionless time  $\tau \equiv \sqrt{La}(t/T)$ . At short times  $\tau \lesssim 3$ ,  $L$  is practically a constant – very few droplets have merged. During the same time interval the kinetic energy of the flow grows as  $E(t) \sim t^2$ . At intermediate times  $10 \lesssim \tau \lesssim 100$  the kinetic energy of the flow remains almost a constant (decreases slowly) while the characteristic length scale grows as  $L(t) \sim t^{1/2}$  for at least a decade. We also detect a dependence on Cahn number – the transition to  $L \sim t^{1/2}$  happens earlier for larger Cahn number. At very late times  $100 \lesssim \tau$ , as expected, the kinetic energy starts to decay fast while  $L$  saturates. The scaling of  $L$  with a dynamic exponent of  $1/2$  has been observed before in two-dimensional simulations [36] in the presence of noise and for an off-critical quench but never before in three dimensions [37].

In Fig. (3) we show representative plots of the *compensated* structure factor,  $q^2\mathbb{S}(q)$  and the *compensated* energy spectrum,  $q^{5/3}\mathbb{E}(q)$  for times during which the  $L \sim t^{1/2}$  scaling is observed. In both cases we find a region in  $q$  over which the compensated plots are approximately horizontal. This implies that over this range

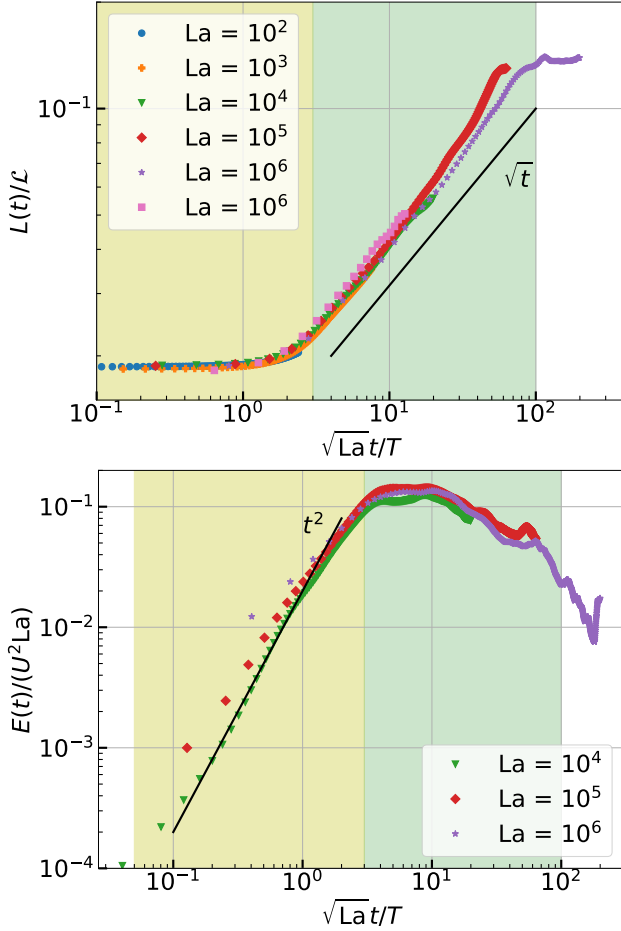


FIG. 2. The evolution of the (A) The characteristic length-scale,  $L(t)$ , and (B) the total kinetic energy  $E(t)$  for all the A runs,  $Sc = 1$ . The data for different Laplace number collapse on each other when plotted as a function of the scaled time  $\tau \equiv \sqrt{Lat}/T$ .

of  $q$ ,

$$\mathbb{S}(q) \sim q^{-2} \quad \text{and} \quad \mathbb{E}(q) \sim q^{-5/3} \quad (4)$$

The change in  $\phi$  across a length scale  $r$ ,  $\delta_r \phi$  has two contributions, one smooth – if  $r$  lies either well inside a droplet or well outside droplets – and the another independent of  $r$  – if  $r$  lies across the boundary of a droplet. In other words, there are isolated jumps connected by smooth regions which implies [38, section 8.5.2], similar to Burgers equation [39],  $\mathbb{S}(q) \sim q^{-2}$ . The scaling  $\mathbb{E}(q) \sim q^{-5/3}$  signifies fully developed turbulence a-la Kolmogorov. This plays a key role in the scaling theory we discuss next.

We construct a scaling theory by generalizing the standard approach [2]. From Eq. (1a) the rate of change of characteristic length scale of a droplet is given by  $\phi dL/dt \sim J$  where  $J \equiv |\mathbf{J}|$ . Let  $\Delta\mu$  be the difference in chemical potential between the two phases. By creating a droplet of size  $L$  we both gain,  $(\phi\Delta\mu(4/3)\pi L^3)$  and loose  $(-4\pi\sigma L^2)$  free energy. Minimizing the change

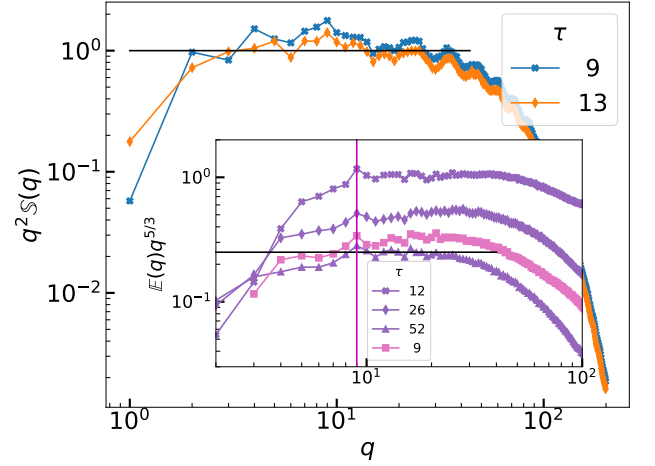


FIG. 3. The compensated structure factor,  $q^2 \mathbb{S}(q)$  as a function of  $q$  in log-log scale at two different times for the run A6 ( $N = 1024$ ). A range of  $q$  over which the compensated plot is flat implies  $\mathbb{S}(q) \sim q^{-2}$  over that range. We plot a horizontal line for comparison. Inset: The compensated kinetic energy spectra,  $q^{5/3} \mathbb{E}(q)$  as a function of  $q$  in log-log scale at three different times for the run A3 ( $N = 512$ ) and at  $\tau = 9$  for the run A6 ( $N = 1024$ ). A range of  $q$  over which the compensated spectra is flat implies  $\mathbb{E}(q) \sim q^{-5/3}$  over that range. We plot a horizontal line for comparison. The compensated spectra has a peak at  $q = q_* \approx 9$  shown by a vertical line. Note that  $q_*$  does not change with time.

in free-energy we estimate  $\Delta\mu \approx 2\sigma/(L\phi)$ . Typical gradients of chemical potential can then be estimated as  $\nabla\mu \sim \Delta\mu/L \sim 2\sigma/(\phi L^2)$ . We assume that at all times the diffusive contribution to the flux,  $J$ , in Eq. (1b) is negligible compared to the advective contribution. In addition, at short times the flow velocities are so small that Eq. (1) reduces to,

$$\frac{dL}{dt} \approx 0 \quad \text{and} \quad \partial_t \mathbf{v} \approx \phi \nabla \mu \sim 2 \frac{\sigma}{L^2}. \quad (5)$$

Then at short times  $L(t)$  remains almost a constant and  $E(t) \sim t^2$  – this rationalizes the short-time behaviour in Fig. (2B).

At intermediate times and at large scales the contribution from the nonlinear term dominates over the viscous term in the momentum equation, Eq. (1f), such that

$$\frac{dL}{dt} \approx \phi v \quad \text{and} \quad \rho \mathbf{v} \cdot \nabla \mathbf{v} \sim \phi \nabla \mu \quad (6)$$

Next we assume that  $\ell$  is the characteristic length scale of the flow. If  $\ell$  is proportional to the scale of droplet,  $L$ ,  $v \sim \sqrt{\sigma/(\rho L)}$ ; consequently  $\sqrt{L} dL/dt \sim \sqrt{\sigma/\rho}$ , which in turn implies  $L \sim t^{2/3}$  – Furukawa’s scaling [23]. Crucially, if  $\ell$  is different from  $L$  and is almost a constant at intermediate times we obtain  $L dL/dt \sim \sqrt{2\sigma\ell/\rho}$ , which implies  $L \sim \sqrt{t}$ .

Let us now critically examine our theory. First, we assume the advective flux dominates over the diffusive flux

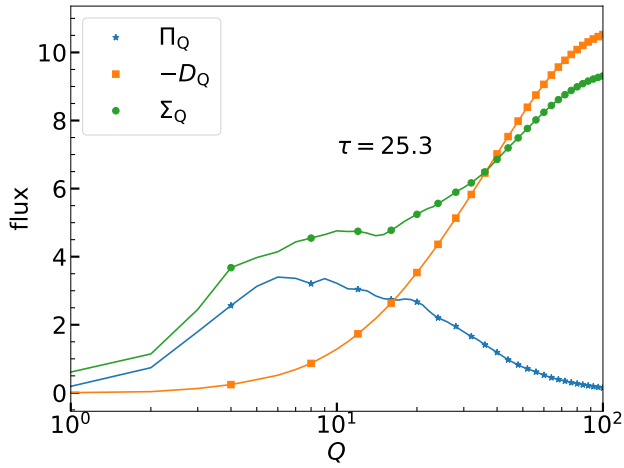


FIG. 4. The three terms on the right hand side of the energy flux equation (8) at an intermediate time  $\tau = 25.3$ .

in Eq. (1b). We find that this is true in our simulations at all times [40].

Second, at intermediate times ( $10 \lesssim \tau \lesssim 100$ ) and at large length scales the nonlinear term in Eq. (1f): (a) dominates over the viscous term; (b) has a characteristic length scale,  $\ell$ , different from the scale  $L$ ; and (c) the length scale  $\ell$  is almost a constant over the timescale. If (a) holds then at large scales the flow must be turbulent and obeys Kolmogorov theory [38], i.e., there must exist a range of wavevectors  $q$  over which  $\mathbb{E}(q) \sim q^{-5/3}$ . This is indeed what we have already shown in Fig. (3). Furthermore we notice that the spectra at large scale has a characteristic peak near  $q = q_* \approx 9$  (marked by a vertical line in the inset of Fig. (3)). The location of this peak,  $q_*$  does not change with time. Hence we can define the characteristic length scale of the flow to be  $\ell = 2\pi/q_*$  – this scale remains almost a constant during the intermediate times. This confirms both (b) and (c) above.

To directly examine the relative importance of the terms in the momentum equation Eq. (1f) it is usual [38] to examine the scale-by-scale energy budget in the Fourier space, defined by

$$\mathcal{E}_Q = \frac{1}{2} \int_0^Q dq \int \mathbb{E}(q) \quad . \quad (7)$$

Straightforward algebra starting from Eq. (1f) shows

$$\partial_t \mathcal{E}_Q = \Pi_Q + D_Q - \Sigma_Q \quad (8)$$

where  $\Pi_Q$ ,  $D_Q$  and  $\Sigma_Q$  are contributions from the non-linear term, the viscous term, and the  $\phi \nabla \mu$  in Eq. (1f), respectively [41]. The viscous term  $D_Q$  is always negative whereas both  $\Pi_Q$  and  $\Sigma_Q$  can, in principle, have either signs. A positive  $\Pi_Q$  implies that the kinetic energy cascades from large to small length scales which is the case of Kolmogorov turbulence in three dimensions. The contribution from surface tension  $\Sigma_Q$ , is positive when coagulation of droplets releases free energy that drives the

fluid and negative when the flow drives droplet motion. At short times,  $\tau \lesssim 3$ , as expected, we find that both  $\Pi_Q$  and  $D_Q$  are small compared to  $\Sigma_Q$  [42], hence (8) reduces to  $\partial_t \mathcal{E}_Q \approx \Sigma_Q$  – supporting the dominant balance assumed in (5). This implies  $E(t) = \lim_{Q \rightarrow \infty} \mathcal{E}_Q \sim t^2$  – the same scaling we find in Fig. (2B). At intermediate times, for large length scale (small enough  $Q$ ,  $Q < 10$ ) the contribution from  $\phi \nabla \mu$  is largely balanced by the non-linear term, see Fig. (4). Consequently, the dominant balance in (8) is  $\Sigma_Q \approx \Pi_Q$  justifying (6).

Note that turbulence in Cahn–Hilliard–Navier–Stokes equation has been studied extensively but also exclusively with an external stirring force generating and maintaining the turbulence [5, 35, 43–46]. By contrast, in our case the turbulence is generated by coagulating droplets. The spectra for both velocity and the phase-variable,  $\phi$ , shows power-law scaling, i.e., they are scale invariant. Hence each possess only two characteristic length scales, respectively, the large scale and small scale cutoffs of the scaling which are often called the integral scale and the dissipative scale [47]. We use  $Sc = 1$ , consequently the small scale cutoffs are practically the same. But the large scale cutoffs are very different.

Two related problem are *pseudo-turbulence* – turbulence generated by rising bubbles [48–51] in a quiescent fluid – and stirred Kolmogorov turbulence modified by rising bubbles [48, 52–54]. In both of these cases, coagulation plays negligible role and the effect of the bubbles give rise to the kinetic energy spectrum  $\mathbb{E}(q) \sim q^{-3}$  [55] that can be understood by balancing the energy production by the bubbles with the viscous dissipation [48, 50, 53, 54]. Our simulations corresponds to a very different parameter range where the contribution due to the chemical potential balances the advective nonlinearity.

It has been emphasized before [56] that coarsening of the domains in phase-separating binary fluids is not scale-invariant – different characteristic length scales constructed from  $\phi$  scales differently. Note that we focus on a very different aspect – we consider only the integral scale, defined in (3), and show that it scales as  $L \sim t^{1/2}$  at intermediate times during which the characteristic length scale of the flow remains almost the same.

In conclusion, we explore the coarsening phenomena at small diffusivity and viscosity in that part of the phase diagram where droplet spinodal decomposition operates. We find turbulence a-la Kolmogorov and emergence of very different characteristic scales of the droplets and the flow – general scale invariance is broken – the integral scale of the droplets  $L \sim t^{1/2}$  where the characteristic scale of the flow remains practically constant. Nevertheless, we are able to generalize the standard scaling theory to the present case and obtain clear agreement between theory and simulations. The key to understand the problem is to calculate the scale-by-scale energy budget.

## ACKNOWLEDGMENTS

The figures in this paper are plotted using the free software matplotlib [57] and VisIt [58]. This work is partially funded by the “Bottlenecks for particle growth in turbulent aerosols” grant from the Knut and Alice Wallenberg Foundation (2014.0048). PP acknowledges support from the Department of Atomic Energy (DAE), India under Project Identification No. RTI 4007,

and DST (India) Project Nos. ECR/2018/001135 and DST/NSM/R&D\_HPC\_Applications/2021/29. DM acknowledges the support of the Swedish Research Council Grant No. 638-2013-9243 as well as 2016-05225. The simulations were performed on resources provided by the Swedish National Infrastructure for Computing (SNIC) at PDC center for high performance computing. We particularly thank Tor Kjellsson and Harald Barth for their help with visualization.

- 
- [1] P. C. Hohenberg and B. I. Halperin, “Theory of dynamic critical phenomena,” *Rev. Mod. Phys.* **49**, 435 (1977).
  - [2] P.M. Chaikin and T.C. Lubensky, *Principles of condensed matter physics* (Cambridge, Cambridge University Press, UK, 1998).
  - [3] Michael E Cates and Martin R Evans, *Soft and fragile matter: nonequilibrium dynamics, metastability and flow (PBK)* (CRC Press, 2000).
  - [4] Alan J Bray, “Theory of phase-ordering kinetics,” *Advances in Physics* **51**, 481–587 (2002).
  - [5] Akira Onuki, *Phase transition dynamics* (Cambridge University Press, 2002).
  - [6] ME Cates, “Complex fluids: the physics of emulsions,” *Soft Interfaces: Lecture Notes of the Les Houches Summer School: Volume 98, July 2012* **98**, 317 (2017).
  - [7] Michael E Cates and Elsen Tjhung, “Theories of binary fluid mixtures: from phase-separation kinetics to active emulsions,” *Journal of Fluid Mechanics* **836** (2018).
  - [8] James K Hoffer and Dipen N Sinha, “Dynamics of binary phase separation in liquid  $^3\text{He}$ - $^4\text{He}$  mixtures,” *Physical Review A* **33**, 1918 (1986).
  - [9] Johannes Hofmann, Stefan S Natu, and S Das Sarma, “Coarsening dynamics of binary bose condensates,” *Physical review letters* **113**, 095702 (2014).
  - [10] JT Mendonça and R Kaiser, “Photon bubbles in ultracold matter,” *Physical review letters* **108**, 033001 (2012).
  - [11] Philippe Chomaz, Maria Colonna, and Jørgen Randrup, “Nuclear spinodal fragmentation,” *Physics reports* **389**, 263–440 (2004).
  - [12] D Boyanovsky, HJ De Vega, and DJ Schwarz, “Phase transitions in the early and present universe,” *Annu. Rev. Nucl. Part. Sci.* **56**, 441–500 (2006).
  - [13] KH Prendergast and EA Spiegel, “Photon bubbles,” *Comments on Astrophysics and Space Physics* **5**, 43 (1973).
  - [14] M Rieutord, B Dubrulle, and EA Spiegel, “Phenomenological photofluidynamics,” *European Astronomical Society Publications Series* **21**, 127–145 (2006).
  - [15] John W Cahn and John E Hilliard, “Free energy of a nonuniform system. i. interfacial free energy,” *The Journal of chemical physics* **28**, 258–267 (1958).
  - [16] François Leyvraz, “Scaling theory and exactly solved models in the kinetics of irreversible aggregation,” *Physics Reports* **383**, 95–212 (2003).
  - [17] Ilya M Lifshitz and Vitaly V Slyozov, “The kinetics of precipitation from supersaturated solid solutions,” *Journal of physics and chemistry of solids* **19**, 35–50 (1961).
  - [18] C Wagner, “Theory of the aging of precipitates by dissolution-reprecipitation (ostwald ripening),” *Z Elektrochem* **65**, 581–11 (1961).
  - [19] Kurt Binder and D Stauffer, “Theory for the slowing down of the relaxation and spinodal decomposition of binary mixtures,” *Physical Review Letters* **33**, 1006 (1974).
  - [20] Eric D Siggia, “Late stages of spinodal decomposition in binary mixtures,” *Physical review A* **20**, 595 (1979).
  - [21] Maxi San Miguel, Martin Grant, and James D Gunton, “Phase separation in two-dimensional binary fluids,” *Physical Review A* **31**, 1001 (1985).
  - [22] Hajime Tanaka, “Coarsening mechanisms of droplet spinodal decomposition in binary fluid mixtures,” *The Journal of chemical physics* **105**, 10099–10114 (1996).
  - [23] Hiroshi Furukawa, “Effect of inertia on droplet growth in a fluid,” *Physical Review A* **31**, 1103 (1985).
  - [24] Francis J Alexander, Shiyi Chen, and Daryl W Grunau, “Hydrodynamic spinodal decomposition: Growth kinetics and scaling functions,” *Physical Review B* **48**, 634 (1993).
  - [25] Vivien M Kendon, Michael E Cates, Ignacio Pagonabarraga, J-C Desplat, and Peter Bladon, “Inertial effects in three-dimensional spinodal decomposition of a symmetric binary fluid mixture: a lattice boltzmann study,” *Journal of Fluid Mechanics* **440**, 147–203 (2001).
  - [26] James E Farrell and Oriol T Valls, “Growth kinetics and domain morphology after off-critical quenches in a two-dimensional fluid model,” *Physical Review B* **43**, 630 (1991).
  - [27] Charu Datt, Sumesh P Thampi, and Rama Govindarajan, “Morphological evolution of domains in spinodal decomposition,” *Physical Review E* **91**, 010101 (2015).
  - [28] Ryotaro Shimizu and Hajime Tanaka, “A novel coarsening mechanism of droplets in immiscible fluid mixtures,” *Nature communications* **6**, 1–11 (2015).
  - [29] Ya-Chang Chou and Walter I Goldburg, “Phase separation and coalescence in critically quenched isobutyric acid—water and 2, 6-lutidine—water mixtures,” (1979).
  - [30] Ning-Chih Wong and Charles M Knobler, “Light-scattering studies of phase separation in isobutyric acid+water mixtures: Hydrodynamic effects,” *Physical Review A* **24**, 3205 (1981).
  - [31] F Perrot, P Guenoun, T Baumberger, D Beysens, Y Garrabos, and B Le Neindre, “Nucleation and growth of tightly packed droplets in fluids,” *Physical review letters* **73**, 688 (1994).
  - [32] Md Mahmudur Rahman, Willis Lee, Arvind Iyer, and Stuart J Williams, “Viscous resistance in drop coalescence,” *Physics of Fluids* **31**, 012104 (2019).
  - [33] Aurore Naso and Lennon Ó Náraigh, “A flow-pattern map for phase separation using the navier-stokes–

- cahn-hilliard model,” *European Journal of Mechanics-B/Fluids* **72**, 576–585 (2018).
- [34] A comprehensive description of the algorithm, the complete list of parameters and the non-dimensional equations are given in Appendix A 1. A comparison of our parameters with Ref. [33] and Ref. [25] is given in Appendix A 1 d.
- [35] Prasad Perlekar, Roberto Benzi, Herman JH Clercx, David R Nelson, and Federico Toschi, “Spinodal decomposition in homogeneous and isotropic turbulence,” *Physical review letters* **112**, 014502 (2014).
- [36] Yanan Wu, Francis J Alexander, Turab Lookman, and Shiyi Chen, “Effects of hydrodynamics on phase transition kinetics in two-dimensional binary fluids,” *Physical review letters* **74**, 3852 (1995).
- [37] Ref [59] has found the exponent  $1/2$  for liquid-gas systems, which is similar to model A of Hohenberg and Halperin, but not for binary fluids. Ref. [56] also obtained  $1/2$  but for a length scale that is different from  $L$  for a case with low viscosity where they found that general scale invariance is broken – length scales defined in different ways scale differently. Both of these simulations are in two dimensions.
- [38] U. Frisch, *Turbulence the legacy of A.N. Kolmogorov* (Cambridge University Press, Cambridge, 1996).
- [39] E Aurell, Uriel Frisch, James Lutsko, and M Vergassola, “On the multifractal properties of the energy dissipation derived from turbulence data,” *Journal of Fluid Mechanics* **238**, 467–486 (1992).
- [40] See Appendix A 2.
- [41] Due to the assumption of incompressibility the pressure gradient does not make any contribution.
- [42] See Appendix A 2.
- [43] Ricardo Ruiz and David R Nelson, “Turbulence in binary fluid mixtures,” *Physical Review A* **23**, 3224 (1981).
- [44] Xiang Fan, PH Diamond, L Chacón, and Hui Li, “Cascades and spectra of a turbulent spinodal decomposition in two-dimensional symmetric binary liquid mixtures,” *Physical Review Fluids* **1**, 054403 (2016).
- [45] Samriddhi Sankar Ray and Abhik Basu, “Universality of scaling and multiscaling in turbulent symmetric binary fluids,” *Physical Review E* **84**, 036316 (2011).
- [46] Nairita Pal, Prasad Perlekar, Anupam Gupta, and Rahul Pandit, “Binary-fluid turbulence: Signatures of multifractal droplet dynamics and dissipation reduction,” *Physical Review E* **93**, 063115 (2016).
- [47] Here we ignore the multiscale/multifractal nature of turbulent fluctuations which, to the best of our knowledge, has never been studied in Cahn–Hilliard–Navier–Stokes equations.
- [48] M Lance and J Bataille, “Turbulence in the liquid phase of a uniform bubbly air–water flow,” *Journal of fluid mechanics* **222**, 95–118 (1991).
- [49] Robert F Mudde, “Gravity-driven bubbly flows,” *Annu. Rev. Fluid Mech.* **37**, 393–423 (2005).
- [50] Vivek N Prakash, J Martínez Mercado, Leen van Wijngaarden, Ernesto Mancilla, Yoshiyuki Tagawa, Detlef Lohse, and Chao Sun, “Energy spectra in turbulent bubbly flows,” *Journal of fluid mechanics* **791**, 174–190 (2016).
- [51] Frédéric Risso, “Agitation, mixing, and transfers induced by bubbles,” *Annual Review of Fluid Mechanics* **50**, 25–48 (2018).
- [52] Varghese Mathai, Detlef Lohse, and Chao Sun, “Bubble and buoyant particle laden turbulent flows,” *Annu. Rev. Condens. Matter Phys* **11** (2020).
- [53] Vikash Pandey, Rashmi Ramadugu, and Prasad Perlekar, “Liquid velocity fluctuations and energy spectra in three-dimensional buoyancy-driven bubbly flows,” *Journal of Fluid Mechanics* **884** (2020).
- [54] Vikash Pandey, Dhruvaditya Mitra, and Prasad Perlekar, “Turbulence modulation in buoyancy-driven bubbly flows,” *arXiv preprint arXiv:2105.04812* (2021).
- [55] In bubble-generated-turbulence, typically [48, 53] a  $k^{-3}$  spectrum is observed. In bubble-modified-turbulence, at small wavenumbers a  $k^{-5/3}$  scaling is found which at large wavenumbers crosses over to  $k^{-3}$  scaling [54].
- [56] Alexander J Wagner and JM Yeomans, “Breakdown of scale invariance in the coarsening of phase-separating binary fluids,” *Physical Review Letters* **80**, 1429 (1998).
- [57] J. D. Hunter, “Matplotlib: A 2d graphics environment,” *Computing in Science & Engineering* **9**, 90–95 (2007).
- [58] Hank Childs, Eric Brugger, Brad Whitlock, Jeremy Meredith, Sean Ahern, David Pugmire, Kathleen Biagas, Mark Miller, Cyrus Harrison, Gunther H. Weber, Hari Krishnan, Thomas Fogal, Allen Sanderson, Christoph Garth, E. Wes Bethel, David Camp, Oliver Rübel, Marc Durant, Jean M. Favre, and Paul Navrátil, “VisIt: An End-User Tool For Visualizing and Analyzing Very Large Data,” in *High Performance Visualization—Enabling Extreme-Scale Scientific Insight* (2012) pp. 357–372.
- [59] WR Osborn, E Orlandini, Michael R Swift, JM Yeomans, and Jayanth R Banavar, “Lattice boltzmann study of hydrodynamic spinodal decomposition,” *Physical review letters* **75**, 4031 (1995).
- [60] Lev Davidovich Landau and Evgeny Mikhailovich Lifshitz, *Fluid mechanics*, 2nd ed., *Course of Theoretical Physics*, Vol. 6 (Butterworth–Heinemann, Oxford, UK, 1987) an optional note.

## Appendix A: Supplemental Material

### 1. Model and Method

Here we provide a detailed description of our model, the numerical method and dimensionless parameters for the direct numerical simulation.

#### a. Dynamical equations

We use a phase-field model for binary fluids with a Landau-Ginzburg type  $\phi^4$  free energy. The dynamics is that of a conserved order parameter coupled to an incompressible flow – model H of Hohenberg and Halperin [1] from which the Langevin noise is excluded.

$$(\partial_t + \mathbf{v} \cdot \nabla)\phi = \Gamma \nabla^2 \mu \quad (\text{A1a})$$

$$\mu = \frac{\delta \mathcal{F}}{\delta \phi} \quad (\text{A1b})$$

$$\mathcal{F}[\phi] = \frac{\Lambda}{\xi^2} \int d^d x \left[ f(\phi) + \frac{\xi^2}{2} |\nabla \phi|^2 \right] \quad (\text{A1c})$$

$$f(\phi) = \frac{1}{4} (1 - \phi^2)^2 \quad (\text{A1d})$$

$$(\partial_t + \mathbf{v} \cdot \nabla)\mathbf{v} = \nu \nabla^2 \mathbf{v} - \nabla p - \phi \nabla \mu \quad (\text{A1e})$$

$$\nabla \cdot \mathbf{v} = 0 \quad (\text{A1f})$$

As the density of the fluid is constant, we have set it to unity.

#### b. Dimensionless parameters

We choose the radius of the droplets,  $R$ , as our characteristic length scale. There is no characteristic velocity scale set by the initial condition, hence, similar to what is done in convection [60], we use  $\nu/R$ , where  $\nu$  is the viscosity, as our characteristic velocity scale to obtain:

$$(\partial_t + \mathbf{v} \cdot \nabla)\phi = \frac{1}{\text{Sc}} \nabla^2 \mu, \quad (\text{A2a})$$

$$(\partial_t + \mathbf{v} \cdot \nabla)\mathbf{v} = \nabla^2 \mathbf{v} - \nabla p - \frac{\Phi_0^{1/3} \text{La}}{\text{Ch}} \phi \nabla \mu \quad (\text{A2b})$$

Here the four dimensionless numbers are: the Cahn number,  $\text{Ch} \equiv \xi/\mathcal{L}$ , the Schmidt number,  $\text{Sc} \equiv \nu/D$ ; the Laplace number,  $\text{La} \equiv (\sigma R)/\nu^2$ , where  $D \equiv \Gamma \Lambda/\xi^2$ ,  $\sigma = (2\sqrt{2}/3)\Lambda/\xi$  and the initial volume fraction occupied by the heavier phase is  $\Phi_0$ . A different non-dimensionalization [33] gives Reynolds number  $\text{Re} = (3/2\sqrt{2})^{1/2}(\mathcal{L}/R)\sqrt{\text{La}/\text{Ch}}$  and Peclet number  $\text{Pe} = \text{ReSc}$ .

#### c. Numerical algorithm, initial condition, and parameters

Our simulations are done in a cubic box of side  $2\pi$ . This box is discretized in  $N$  equally spaced grid points in each direction. Eq. (1) is solved by using a pseudo-spectral method with one-half dealiasing and periodic boundary conditions. We use a second-order Adams-Bashforth scheme for time stepping. An earlier version of this code has been used before in Ref. [35]. The velocity is zero at  $t = 0$ . Initial conditions for order parameter  $\phi$  are chosen to have an array of droplets as shown in Fig. (1) (B),  $\phi = 1$  inside the drops and  $-1$  outside. Simulation parameters are listed in table I.

#### d. Comparison of our parameters with earlier work

Recently Naso and Naráigh [33] have, for the first time, ventured in to the part of the parameters space with small diffusivity and viscosity and found signatures of novel coarsening behavior in this regime. Their simulations

TABLE I. Parameters of simulations. The simulations are in  $2\pi$  periodic domains in three-dimensions with  $\mathbf{N}^3$ ,  $N = 512$  and 1024 collocation points. All the simulations have  $Sc = 1$ . Initially, we choose all the droplets to have the same radius  $R/\mathcal{L} = 1/(8\pi)$  and their centers placed on a cubic lattice. We then add small random perturbations to the radii of the droplets. The initial volume fraction occupied by the droplets (minority phase) is approximately 0.2 such that  $\langle\phi\rangle = 0.62$ .

Runs	$N$	Ch	La
A0	512	0.19	$10^2$
A1	512	0.19	$10^3$
A2	512	0.19	$10^4$
A3	512	0.19	$10^5$
A4	512	0.19	$10^6$
A5	512	0.05	$10^6$
A6	1024	0.1	$10^6$

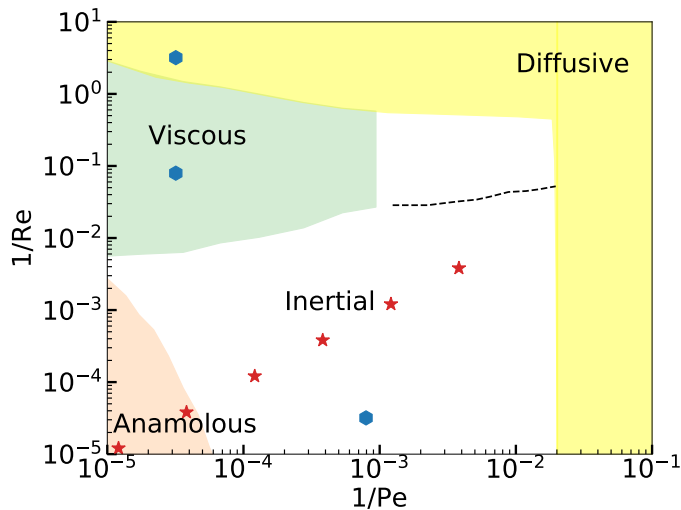


FIG. 5. The phase diagram in the  $1/Pe$ – $1/Re$  plane according to Ref. [33]. The points marked by red star are our simulations. We have also used our code to simulate the system with symmetric initial condition for the points marked in blue and have obtained results that agree with Ref. [33].

started with symmetric initial condition whereas we start with droplets organized on a lattice with defects in the droplet-spinodal regime.

Nevertheless it is useful to compare the dimensionless parameters of our simulations with theirs. Ref. [33] worked with dimensionless viscosity ( $1/Re$ ) and diffusivity ( $1/Pe$ ) and separated the parameters in different phases depending on the types of structures that were observed, not based on the dynamic scaling exponent. Our runs belong to the region on phase space Ref. [33] called “anomalous” and “inertial”. In the notation of Ref. [33] the Cahn–Hilliard–Navier–Stokes equations are:

$$\rho D_t \mathbf{u} = \eta \nabla^2 \mathbf{u} - \nabla P - \phi \nabla \mu, \quad (\text{A3})$$

$$D_t \phi = \frac{D}{\alpha} \nabla^2 \mu, \quad (\text{A4})$$

$$\mu = \alpha(-\phi + \phi^3 - \xi^2 \nabla^2 \phi) \text{ with } \alpha \equiv \frac{\Lambda}{\xi^2}. \quad (\text{A5})$$

Choosing the velocity scale as  $U \equiv \sqrt{\alpha/\rho}$ , the length scale  $\mathcal{L}$  (box size) we obtain the following dimensionless

equations

$$\rho D_t \mathbf{u} = \frac{1}{\text{Re}} \nabla^2 \mathbf{u} - \nabla P - \phi \nabla \mu, \quad (\text{A6})$$

$$D_t \phi = \frac{1}{\text{Pe}} \nabla^2 \mu, \quad (\text{A7})$$

$$\mu = (-\phi + \phi^3 - \text{Ch}^2 \nabla^2 \phi), \quad (\text{A8})$$

with  $\Re \equiv U\mathcal{L}/\nu$ ,  $\text{Ch} = \xi/\mathcal{L}$  and  $\text{Pe} = U\mathcal{L}/D$ ; the Reynolds number, the Cahn number and Peclet number respectively, see Table II.

TABLE II. Dimensionless numbers for our runs. Based on the values of  $1/\text{Pe}$  and  $1/\text{Re}$ , we are in the anomalous regime of Ref. [33].

Run	$D$	$\Lambda$	$\xi$	$\nu$	Ch	Pe	Re
A0	$5 \cdot 10^{-4}$	$2.6 \cdot 10^{-2}$	$2.45 \cdot 10^{-2}$	$5 \cdot 10^{-4}$	$3.9 \cdot 10^{-3}$	$8.27 \cdot 10^3$	$8.27 \cdot 10^3$
A1	$5 \cdot 10^{-4}$	$2.6 \cdot 10^{-3}$	$2.45 \cdot 10^{-2}$	$5 \cdot 10^{-4}$	$3.9 \cdot 10^{-3}$	$2.62 \cdot 10^3$	$2.62 \cdot 10^3$
A2	$5 \cdot 10^{-4}$	$2.6 \cdot 10^{-4}$	$2.45 \cdot 10^{-2}$	$5 \cdot 10^{-4}$	$3.9 \cdot 10^{-3}$	$8.27 \cdot 10^4$	$8.27 \cdot 10^4$
A3	$5 \cdot 10^{-4}$	$2.6 \cdot 10^{-5}$	$2.45 \cdot 10^{-2}$	$5 \cdot 10^{-4}$	$3.9 \cdot 10^{-3}$	$2.61 \cdot 10^4$	$2.61 \cdot 10^4$

## 2. Fluxes

The standard approach to understand scaling behaviour in turbulence is to calculate the scale-by-scale energy budget equation [38]. Here we follow the procedure outline in [35]. Multiplying (A1a) by  $\hat{\phi}(-\mathbf{q})$  and integrating over all the fourier modes upto wave-number  $Q$ , we obtain

$$\partial_t \mathcal{S}_Q + \mathcal{A}_Q = \mathcal{G}_Q \quad (\text{A9})$$

where  $\mathcal{A}_Q$  is the contribution from the advective term and  $\mathcal{G}_Q$  is the contribution from the diffusive term. In particular,

$$\mathcal{A}_Q \equiv \Re \left\{ \int_0^Q \int_{\Omega} \hat{\phi}(-\mathbf{q}) [\widehat{\mathbf{v} \cdot \nabla \phi}](\mathbf{q}) d\mathbf{q} d\Omega \right\}, \quad (\text{A10a})$$

$$\mathcal{G}_Q \equiv \Re \left\{ \Gamma \int_0^Q \int_{\Omega} \hat{\phi}(-\mathbf{q}) [\widehat{\nabla^2 \mu}](\mathbf{q}) d\mathbf{q} d\Omega \right\}. \quad (\text{A10b})$$

In Fig. (6) we show two representative plots of these two fluxes as a function of the wavenumber  $Q$ , one at short times and the other at intermediate times. We find that in all cases and at all  $Q$ , except for very high  $Q$ , the advective flux dominates over the diffusive contribution.

By multiplying the Fourier transformed Eq. (A1e) with  $\hat{\mathbf{v}}(-\mathbf{q})$ , and integrating over all the fourier modes upto wave-number  $Q$ , we obtain

$$\partial_t \mathcal{E}_Q = \Pi_Q + D_Q - \Sigma_Q. \quad (\text{A11})$$

Here  $\mathcal{E}_Q$  is the cumulative kinetic energy. The rest of the quantities in (A11) are defined as follows:

$$\Pi_Q \equiv -\Re \left\{ \int_0^Q \int_{\Omega} \hat{\mathbf{v}}(-\mathbf{q}) \cdot [\widehat{\mathbf{v} \cdot \nabla \mathbf{v}}](\mathbf{q}) d\mathbf{q} d\Omega \right\} \quad (\text{A12a})$$

$$D_Q \equiv -\nu \int_0^Q q^2 \mathbb{E}(q) dq \quad (\text{A12b})$$

$$\Sigma_Q \equiv \Re \left\{ \int_0^Q \int_{\Omega} \hat{\mathbf{v}}(-\mathbf{q}) \cdot [\widehat{\phi \nabla \mu}](\mathbf{q}) d\mathbf{q} d\Omega \right\} \quad (\text{A12c})$$

In Fig. (7) we show a representative plot of all the three contributions on the right hand side of (A11) at short times. Clearly  $\Sigma_Q$  dominates over the other two. Hence we conclude that the system is not in a stationary state – the growth of kinetic energy is fuelled by the contribution from  $\phi \nabla \mu$ .

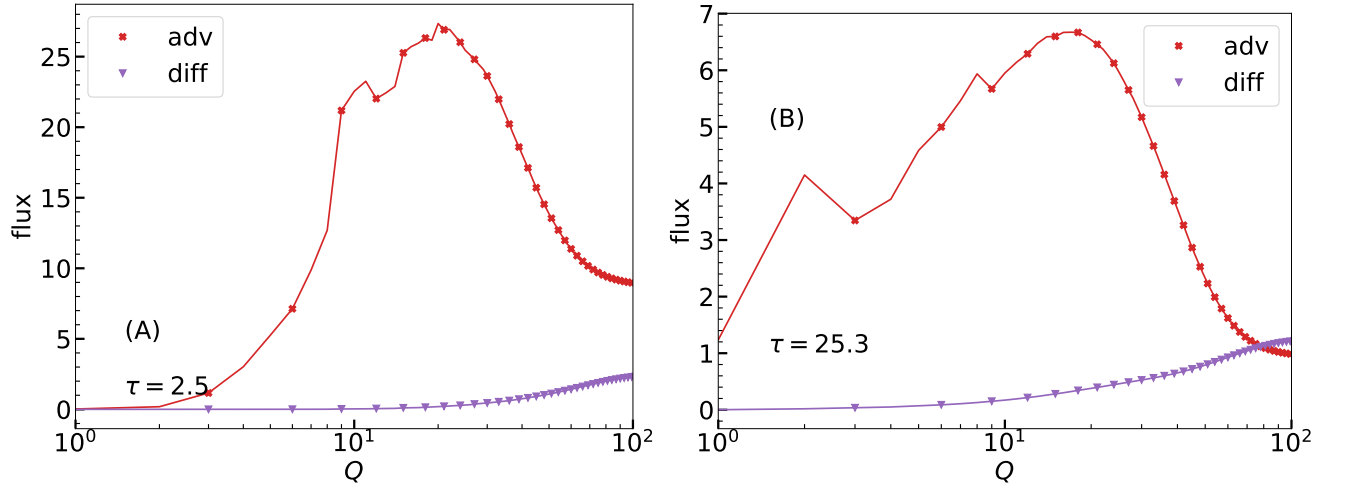


FIG. 6. Contribution to the flux of  $\phi$  from the advective ( $\mathbf{v} \cdot \nabla \phi$ ) and the diffusive ( $\Gamma \nabla^2 \mu$ ) term at early times (A) and intermediate times (B).

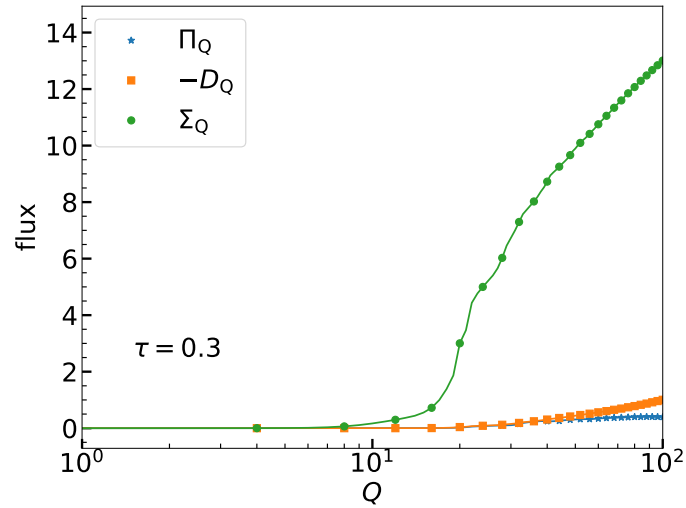


FIG. 7. Contribution to the flux of energy from the nonlinear term ( $\Pi_Q$ ), the viscous term ( $D_Q$ ) and surface tension ( $\Sigma_Q$ ) at early time.